

Modelling and Control of Photovoltaic-Based Microgrid

Ashraf Khalil^{*‡}, Khalid Ateea^{*}

^{*}Electrical and Electronic Engineering Department, Faculty of Engineering, University of Benghazi

(ashraf.khalil@uob.edu.ly, khaledatia.elfitory@gmail.com)

[‡]Corresponding Author; Ashraf Khalil; Khalid Ateea, University of Benghazi - Garyounis, Tel: +218916246520, Fax: +90 312 123 4567,ashraf.khalil@uob.edu.ly

Received: 09.05.2015 Accepted:15.06.2015

Abstract- This paper presents the modelling and control of PV-based Microgrid. Renewable energy sources such as PV, wind and fuel cells are usually connected through voltage-source inverters. In order to share the same loads these inverters are connected in parallel to form a Microgrid. The system considered in the paper consists of two parallel inverters each fed with PV array. As the PV array is variable nonlinear DC source the control system should achieve good power sharing even with this imperfections. The controller is designed in the dq reference frame where the Space Vector Pulse Width Modulation is used. The first inverter controller contains outer voltage control loop and inner current control loop while the second inverter controller contains only power control loop. The controller is tested through simulation where each inverter is fed through PV array with different radiation level. The simulation results show that the power sharing is achieved even when the DC sources are different and nonlinear.

Keywords- parallel inverter; stability; microgrid; photovoltaic; SVPWM.

1. Introduction

Humanity has relied on fossil fuel in the last few hundred years. The ever growing increased energy demands and the energy-related environmental problems of fossil fuel made the renewable energy one of the most viable alternatives for the large centralized fossil-fuelled power plants. Recently distributed energy sources, such as fuel cells, wind turbines and photovoltaic cells are increasingly being used. Most of the renewable energy sources are usually equipped with DC/AC inverters which form a system of parallel inverters that can be connected to the grid. This configuration is known as Microgrid [1]. A Microgrid can be defined as a cluster of microsources, storage systems and loads which may be isolated (stand-alone) or connected to the grid as a single entity as shown in Fig 1. The Microgrid technology is proved to be one of the promising solutions that can cope with the increased energy demands and the negative environmental effects of fossil-fuelled power plants. Distributed power sources in Microgrid must operate in parallel in order to share the loads. Among renewable energy sources, wind and photovoltaic (PV) systems are smaller and more scalable than central power plants which made them suitable to be integrated generators into Microgrid. Photovoltaic System (PV) is one of the exciting new technologies to convert sunlight directly into electricity. According to the learning curve the cost reduction of PV system will continue in the future [2]. PV-Based Microgrid is proven to be one of the forms of future evolution of Libyan grid. In PV-Based Microgrid each PV source is connected to

a DC/AC inverter which must operate in parallel to share the same load.

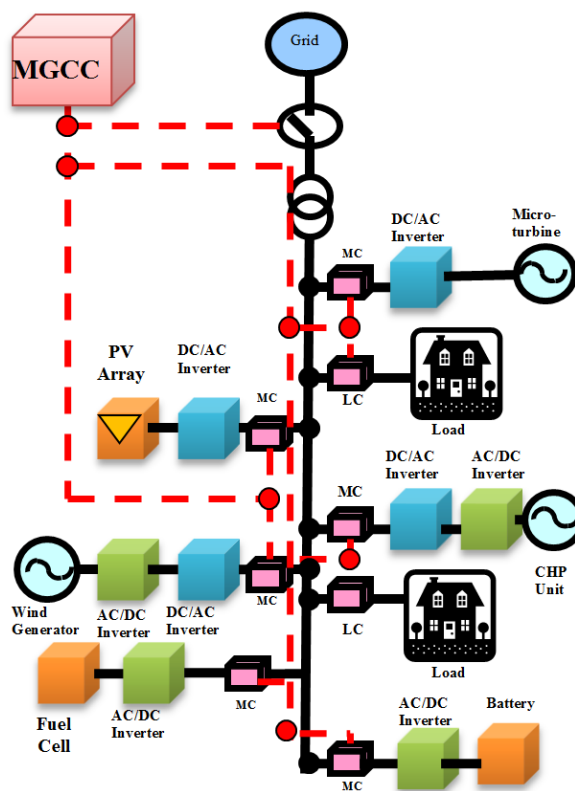


Fig. 1 Inverter-Based Microgrid

The PV source is a series and parallel connections of PV modules. PV modules can be connected to the grid in different configurations such as the central, string and multistring. Due to its low cost and its simplicity the centralized configuration is used for large installations where the PV array is connected to a central inverter. Then these inverters are connected in parallel and hence a control strategy is necessary to stabilize the system and to achieve good power sharing while maintains the voltage and the frequency within predetermined range. Also the controller must achieve synchronization between inverters

There are many reviews on the control strategies in Inverter-based Microgrids (see [3], [4], [5] and the references therein). The control strategies can be classified into centralized, distributed, master-slave and decentralized control strategies [3]. In the centralized control strategy, all the information is sent to a central controller and then the commands are sent back to the system. In this control strategy all the inverters work as current sources and the voltage is controlled in the central controller. The main advantage is that the current sharing is forced at all times even during transient, and different power rating inverters can be connected without changing the control structure [3]. Also the system maintenance can be carried out easily. The main disadvantage of this strategy is the single point of failure and the need for sending the reference voltage to all the inverters in the network, which requires high bandwidth communication link, and the system is sensitive to nonlinear loads [3].

The decentralized control is used to solve the problems associated with the controller's interactions. The decentralized controller relies only on local information and there is no need to send the information to a central controller. This technique usually used when the distance between parallel inverters is long, and can be applied in islanded mode or grid connected mode. One of the widely used decentralized control is the Droop control [4]. The main idea is to regulate the voltage and the frequency by regulating the reactive and the active power respectively that can be sensed locally. The Droop control method has many desirable features such as expandability, modularity, redundancy, and flexibility. There are as well some drawbacks such as, slow transient response and possibility of circulating currents. As the interconnections are neglected the overall system stability cannot guaranteed.

The master slave control strategy is classified as a quasi-decentralized control strategy that can be a compromise between the centralized and the decentralized control strategies. In the master-slave control strategy, one of the converters is known to be the master while the others are the slaves, the master controller contains the voltage controller while the slaves contain current controllers and have to track the master's reference current [5]. Master/Slave control strategy gives a good load sharing and synchronization.

In the distributed control strategy the rotational reference frame (dq_0) is used instead of the stationary reference frame (abc). It can be used only in balanced systems. The voltage

controller controls the output voltage by setting the average current demands [3]. In current/power sharing control method the average unit current can be determined by measuring the total load current and divide this current by the number of units in the system. There are excellent features of the current/power sharing, the load sharing is forced during transient and the circulating currents are reduced. Additionally lower-bandwidth communication link is needed. For these reasons distributed control strategy is adopted in this paper.

With the advances in network technology, shared networks such as the Ethernet, industrial Ethernet and even Internet, are promising as alternative for direct control signals exchange. The shared networks reduces the complexity of wiring and increases system reliability. In this sense control strategies can be classified based on the type of communication exchange between the controllers. Then the control strategies are divided into communication based or communication-less. Many researchers reported master-slave and distributed control strategies that rely on shared-network for control signals exchange [6, 7 and 8].

The paper starts from the description of the PV-based Microgrid. Then the mathematical model of the parallel inverters and the PV array is presented. The PV array is a series and parallel connection of PV modules. The model of the module is the single diode five parameters model. The PV module model is implemented in Matlab/Simulink and the effect of the radiation and the temperature on the PV characteristics is studied through simulation. The distributed control strategy is briefly explained where the space vector pulse width modulation is used. One of the main issues in inverter based Microgrid is the stability of the system. The controller parameters are selected to stabilize the parallel inverters and achieve good performance. A simulation using Matlab/Simpower toolbox is carried out to test the effectiveness of the control strategy when the PV arrays receive different radiation.

2. Mathematical Model of PV-Based Microgrid

The typical circuit of two parallel three-phase voltage source inverters fed through two PV arrays is shown in Fig. 2. The average state-space model is usually used in the analysis of power converters.

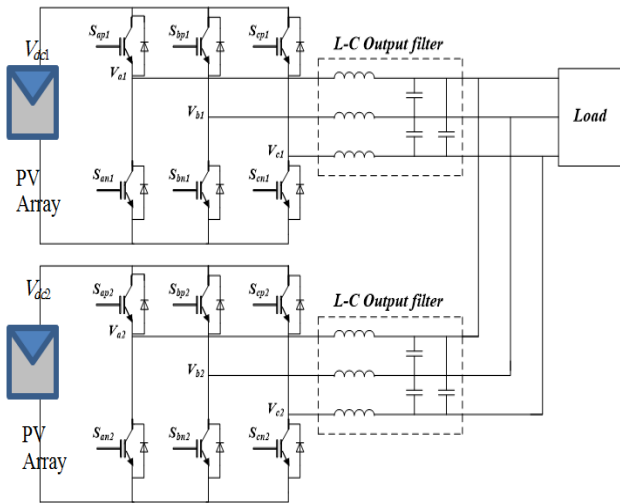


Fig. 2. Two parallel inverters

Each of the parallel inverters is connected to a 10 kW_p PV array. The controller has to stabilize the system and to have a good power sharing even when the sources have different DC values. This is the situation when the arrays receive different radiation because of the shadow or when the two arrays are not alike.

2.1. The Mathematical Model of the PV Array

PV solar cells are made from semiconductor material and rely on the photoelectric effect to generate electricity. The most widely used semiconductor for terrestrial applications is the silicon. PV cells can be made from silicon in three different forms; crystalline silicon, multicrystalline and amorphous silicon. Crystalline silicon PV cells are the most efficient and the most expensive among silicon PV cells. The high production cost of crystalline PV cells is because the process of crystal growth which is slow and consumes energy. On the other hand amorphous PV cells are less efficient and the cost is lower because of their inexpensive method of production. Microcrystalline silicon PV cells are compromise between the cost and the efficiency. The efficiency is important when the area is a key factor because the higher the efficiency, the smaller the area required. The basic PV cell is the p-n junction shown in Fig 3.a. In the dark the characteristics of the PV cell is similar to the normal diode. When sunlight with energy greater than the semiconductor energy gap hits the cell electrons becomes free and a considerable current flows in the external circuit.

As PV cells are fragile and have low voltage they grouped into modules and encapsulated from front and supported by metallic panel for protection. The modules are then connected in series and parallel to form an array as shown in Fig 3.b.

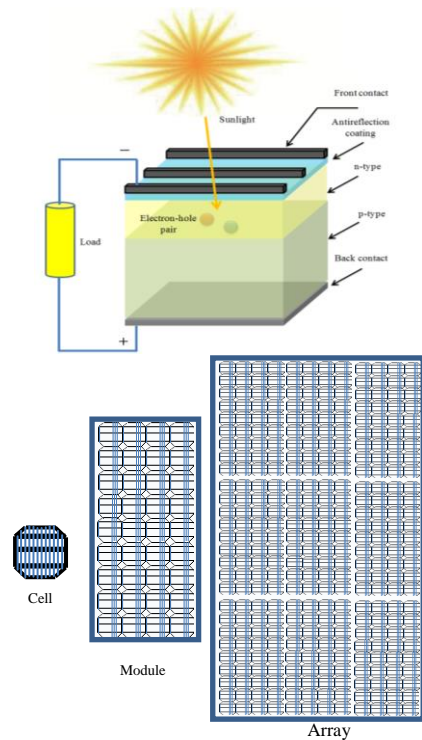


Fig. 3. (a) A pn-junction silicon solar cell, (b) A connections of cells forms a module and a connection of modules forms an array

For PV energy conversion systems the most important parts in their modelling are the IV and PV curves. Many studies focus on modelling the PV cell instead of the PV module. This is not practical because the manufacturer provides the module data not the cell data. In order to obtain the IV and PV curves a mathematical model must be derived. There are many methods in the literature for modelling PV modules [9, 10 and 11]. The model used in this paper is based on the single-diode model and extracting some of the parameters from the manufacturer data sheet. The electrical circuit model is shown in Fig 4.

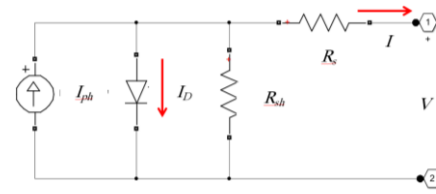


Fig. 4. Circuit model of a solar cell

The model is with middle complexity where the temperature dependence of I_0 , I_{ph} , and V_{oc} are included. Also the parasitic resistances R_s and R_{sh} and their temperature dependence are taken into account. The ideality factor is used as a variable to match the simulated data with the manufacturing data. The mathematical model of a solar cell based on the single diode model is given as:

$$I(T,G,V) = I_{ph} - I_0(e^{(V+IR_s)/nV_{th}} - 1) - (V + I \cdot R_s) / R_{sh} = I_{ph} - I_D - I_{sh} \quad (1)$$

Where the variables in (1) are given by [10];

$$I_{ph} = I_{ph0} \cdot G / G_{nom} \quad (2)$$

$$I_{ph}(T) = I_{ph} + K_0(T - T_{meas}) \quad (3)$$

$$K_0 = (I_{ph}(T_2) - I_{ph}(T_1)) / (T_2 - T) \quad (4)$$

$$I_0 = I_{SC(T_1)} \cdot (T / T_1)^{3/n} \cdot \exp[-E_g / V_s(1/T - 1/T_1)] \quad (5)$$

$$I_0(T_1) = I_{SC(T_1)} / (e^{qV_{OC(T_1)} / nkT_1} - 1) \quad (6)$$

$$R_s(T) = -dV / dI_{V_{OC}} - 1 / (I_0(T_1) \cdot q / nkT_1 \cdot e^{qV_{OC(T_1)} / nkT_1}) \quad (7)$$

$$R_{sh} = V_{OC} / [I_{ph} - I_0(e^{nkT_{meas}} - 1)] \quad (8)$$

$$R_{sh}(T) = R_{sh} \cdot (T / T_{meas})^\alpha \quad (9)$$

The parameters in the model are explained briefly. I_{ph} is the photo generated current in Amperes. I_{ph0} is the photo generated current at the nominal radiation. I_0 is the diode dark saturation current. I_D is the diode dark current. I_{sh} is the shunt current. R_s is the series resistance. R_{sh} is the shunt resistance. G is the solar radiation in W/m^2 . The G_{nom} is the radiation the PV module is calibrated at. n is the ideality factor. e is the electron charge. k is Boltzmann's constant. V_g is the semiconductor energy gap. K_0 is the short-circuit current temperature coefficient. The manufacturer provides the following: N_s is number of cells in series, N_p is the number of cells in parallel, I_{sc} is the short-circuit current, V_{oc} is the open-circuit voltage, K_0 is the short-circuit current temperature coefficient. $V_{th} = nkT_c / e$. The Solarex MSX60 60W module is used in the simulation [12]. The equations from (1) to (9) are implemented in Matlab/Simulink shown in Fig 5.

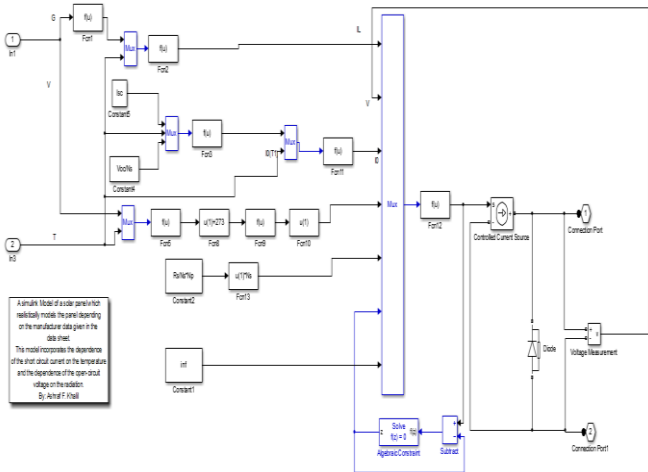


Fig. 5. The Simulink PV model implementation

The masked PV module is shown in Fig 6 along with the mask. The module parameters are shown in Fig. 6. The PV module can be used as circuit element in SimPower/Matlab toolbox and does not need extra interface as the solar cell in Simscape/Matlab Toolbox.

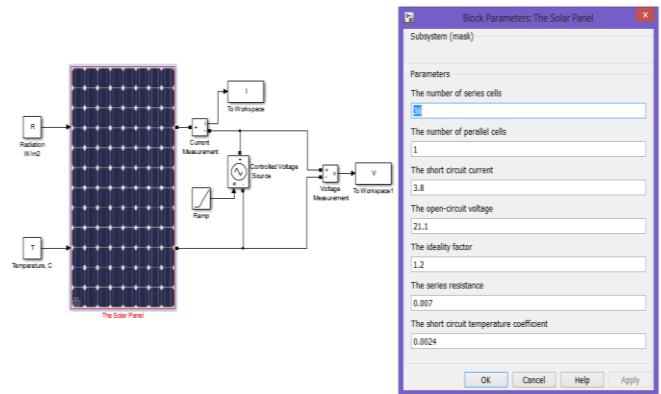


Fig. 6. The PV Simulink model

When the PV module is connected to a load a specific current will flow through the load and a voltage will be built across the load terminals. The IV characteristics are shown in Fig 7 where the radiation is set to $1000 W/m^2$ and the cell temperature is $25 ^\circ C$. When the terminal of the module is short circuited a maximum current flows, this current is known as the short-circuit current. As the load resistance increases the operating point moves to the right and the power increases. At a point called the maximum power point (MPP) the power reaches to its maximum. Increasing the point to the right of the MPP, the load is decreased and the power is reduced. At a very high load resistance the current is zero, the voltage at this point is the open-circuit voltage. In order to harvest maximum power the load should equal R_{mppt} and this is impractical because the weather is keep changing and hence the radiation and the temperature will be changing.

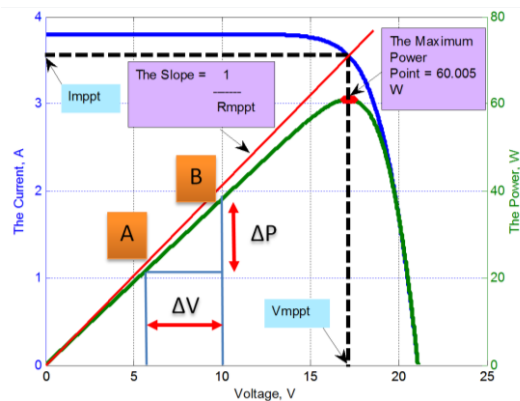


Fig. 7. The IV and PV characteristics

In order to understand the behaviour of the PV module simulations are carried out. The effect of the temperature on the IV and PV characteristics are shown in Fig 8.a and Fig 8.b. The effect of the radiation on the IV and PV characteristics are shown in Fig 8.c and Fig 8.d. It is clear that as the temperature increases the short-circuit current increases slightly while the open-circuit is reduced. The resultant effect is a reduction in the PV module power as the temperature of the cell rises. The radiation has a stronger effect on the characteristics of the PV module. As the radiation is increased the current increases linearly with radiation and the voltage increases logarithmically. The generated power increases as the radiation increases.

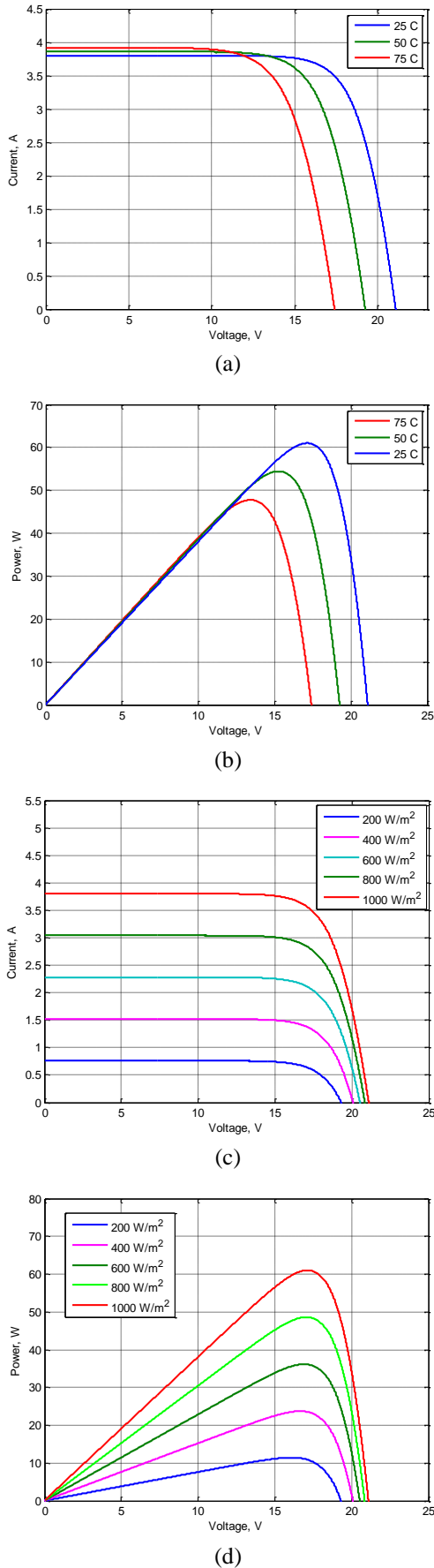


Fig. 8. (a) The effect of the temperature on the IV characteristics, (b) The effect of the temperature on the PV characteristics, (c) The effect of the radiation on the IV characteristics, and (d) The effect of the radiation on the PV characteristics

characteristics, (c) The effect of the radiation on the IV characteristics, and (d) The effect of the radiation on the PV characteristics

There are many configurations for PV system such as the central, string and multi-string. The one used in this paper is the central inverter configuration shown in Fig 9. The PV modules are connected in series and parallel to produce the required voltage and power. The main advantages of this configuration are the low cost, the simplicity and the high efficiency by using single inverter.

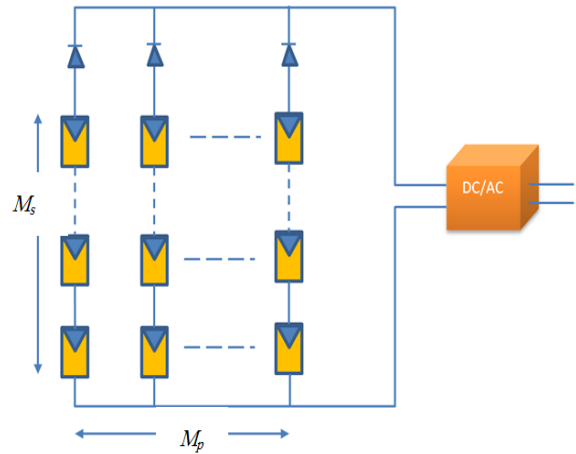


Fig. 9. The PV array is connected to the inverter

As our energy source is nonlinear the goal of the controller is to generate AC power with given voltage shape parameters and to achieve power sharing between the different inverters in the Microgrid. As can be seen from Fig. 9, M_s and M_p stand for the number of series and parallel module to be connected to form the array. The array used in the simulation has 10 branches with 22 modules in each branch and the total number of modules is 220.

2.2. The Mathematical Model of the Parallel Inverters

The average model of the phase leg is derived based on the switching averaging. After transformation of the variables in the stationary coordinates X_{abc} into the rotating coordinates X_{dqz} , the average model can be simplified [13, 14 and 15] based on $i_z = i_{z1} = -i_{z2} \approx 0$:

$$\frac{d}{dt} \begin{bmatrix} i_{d1} \\ i_{q1} \end{bmatrix} = \frac{1}{L_1} \begin{bmatrix} d_{d1} \\ d_{q1} \end{bmatrix} V_{dc1} - \frac{1}{L_1} \begin{bmatrix} v_d \\ v_q \end{bmatrix} - \begin{bmatrix} 0 & -\omega \\ \omega & 0 \end{bmatrix} \cdot \begin{bmatrix} i_{d1} \\ i_{q1} \end{bmatrix} \quad (10)$$

$$\frac{d}{dt} \begin{bmatrix} i_{d2} \\ i_{q2} \end{bmatrix} = \frac{1}{L_2} \begin{bmatrix} d_{d2} \\ d_{q2} \end{bmatrix} V_{dc2} - \frac{1}{L_2} \begin{bmatrix} v_d \\ v_q \end{bmatrix} - \begin{bmatrix} 0 & -\omega \\ \omega & 0 \end{bmatrix} \cdot \begin{bmatrix} i_{d2} \\ i_{q2} \end{bmatrix} \quad (11)$$

$$\frac{d}{dt} \begin{bmatrix} v_d \\ v_q \end{bmatrix} = \frac{1}{2C} \begin{bmatrix} i_{d1} \\ i_{q1} \end{bmatrix} + \frac{1}{2C} \begin{bmatrix} i_{d2} \\ i_{q2} \end{bmatrix} - \frac{1}{RC} \begin{bmatrix} v_d \\ v_q \end{bmatrix} - \begin{bmatrix} 0 & -\omega \\ \omega & 0 \end{bmatrix} \cdot \begin{bmatrix} v_d \\ v_q \end{bmatrix} \quad (12)$$

Assuming that the input DC power sources is ideal:

$$\frac{d}{dt} \begin{bmatrix} \tilde{i}_{d1} \\ \tilde{i}_{q1} \end{bmatrix} = \frac{1}{L_1} \begin{bmatrix} \tilde{d}_{d1} \\ \tilde{d}_{q1} \end{bmatrix} V_{dc1} - \frac{1}{L_1} \begin{bmatrix} \tilde{v}_d \\ \tilde{v}_q \end{bmatrix} - \begin{bmatrix} 0 & -\omega \\ \omega & 0 \end{bmatrix} \cdot \begin{bmatrix} \tilde{i}_{d1} \\ \tilde{i}_{q1} \end{bmatrix} \quad (13)$$

$$\frac{d}{dt} \begin{bmatrix} \tilde{i}_{d2} \\ \tilde{i}_{q2} \end{bmatrix} = \frac{1}{L_2} \begin{bmatrix} \tilde{d}_{d2} \\ \tilde{d}_{q2} \end{bmatrix} V_{dc2} - \frac{1}{L_2} \begin{bmatrix} \tilde{v}_d \\ \tilde{v}_q \end{bmatrix} - \begin{bmatrix} 0 & -\omega \\ \omega & 0 \end{bmatrix} \cdot \begin{bmatrix} \tilde{i}_{d2} \\ \tilde{i}_{q2} \end{bmatrix} \quad (14)$$

$$\frac{d}{dt} \begin{bmatrix} \tilde{v}_d \\ \tilde{v}_q \end{bmatrix} = \frac{1}{2C} \left(\begin{bmatrix} \tilde{i}_{d1} \\ \tilde{i}_{q1} \end{bmatrix} + \begin{bmatrix} \tilde{i}_{d2} \\ \tilde{i}_{q2} \end{bmatrix} \right) - \begin{bmatrix} 1/RC & -\omega \\ \omega & 1/RC \end{bmatrix} \cdot \begin{bmatrix} \tilde{v}_d \\ \tilde{v}_q \end{bmatrix} \quad (15)$$

Writing (13), (14) and (15) in general matrix form:

$$\tilde{\dot{\mathbf{x}}} = \mathbf{A}\tilde{\mathbf{x}} + \mathbf{B}\tilde{\mathbf{u}} \quad (16)$$

$$\tilde{\mathbf{y}} = \mathbf{C}\tilde{\mathbf{x}} \quad (17)$$

The state vector and the control vector are given as:

$$\tilde{\mathbf{x}} = [\tilde{v}_d \quad \tilde{v}_q \quad \tilde{i}_{d1} \quad \tilde{i}_{q1} \quad \tilde{i}_{d2} \quad \tilde{i}_{q2}]^T$$

$$\tilde{\mathbf{u}} = [\tilde{d}_{d1} \quad \tilde{d}_{q1} \quad \tilde{d}_{d2} \quad \tilde{d}_{q2}]^T$$

$\mathbf{C} = \mathbf{I}$, the matrices \mathbf{A} , \mathbf{B} can be obtained as:

$$\mathbf{A} = \begin{bmatrix} -1/RC & \omega & 1/(2C) & 0 & 1/(2C) & 0 \\ -\omega & -1/RC & 0 & 1/(2C) & 0 & 1/(2C) \\ -1/L_1 & 0 & 0 & \omega & 0 & 0 \\ 0 & -1/L_1 & -\omega & 0 & 0 & 0 \\ -1/L_2 & 0 & 0 & 0 & 0 & \omega \\ 0 & -1/L_2 & 0 & 0 & -\omega & 0 \end{bmatrix} \quad (18)$$

$$\mathbf{B} = \begin{bmatrix} 0 & 0 & V_{dc1}/L_1 & 0 & 0 & 0 \\ 0 & 0 & 0 & V_{dc1}/L_1 & 0 & 0 \\ 0 & 0 & 0 & 0 & V_{dc1}/L_1 & 0 \\ 0 & 0 & 0 & 0 & 0 & V_{dc1}/L_1 \end{bmatrix}^T \quad (19)$$

3. The Control Strategy

The distributed control strategy is used where the first and the second inverter have two control loops as shown in Fig. 10. The inner control loops independently regulate the inverter output current in the rotating reference frame, i_d and i_q . The outer loop works in the voltage control mode to produce the d-q axis current references for the inner loop by regulating the voltage at given reference value as shown in Fig 11. In power control mode, the outer loop is used to regulate the active and the reactive power at given operating points and provide the current references, i_{d-ref} and i_{q-ref} , in the rotating reference frame for the inner loop as shown in Fig. 12 ([14] and [15]).

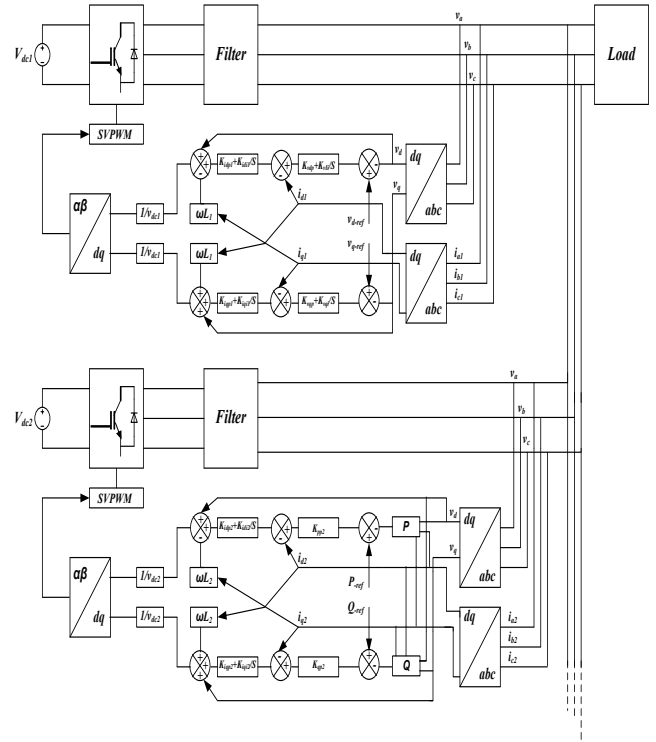


Fig. 10. The distributed control of the two parallel inverters

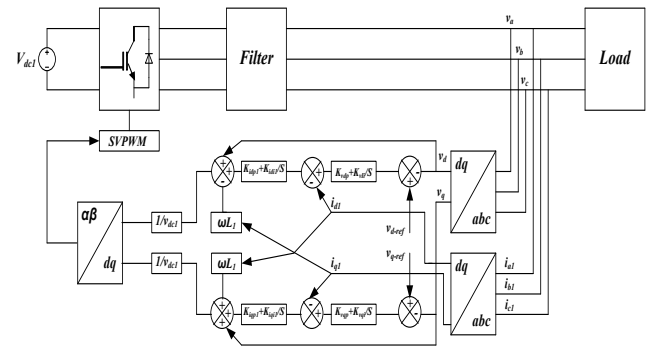


Fig. 11. The first inverter with voltage and current control loop

The Space Vector Pulse Width Modulation (SVPWM) ([14] and [15]) is used to derive the six pulses. A proportional-integral (PI) control scheme is used in both the voltage and control loops, the duty cycles signals are given as:

$$\tilde{d}_{d1} \cdot V_{dc1} = (K_{idp1} + K_{idil}/s) (\tilde{i}_{d1-ref} - \tilde{i}_{d1}) - \omega L_1 \tilde{i}_{q1} + \tilde{v}_d \quad (20)$$

$$\tilde{d}_{q1} \cdot V_{dc1} = (K_{iqp1} + K_{iqil}/s) (\tilde{i}_{q1-ref} - \tilde{i}_{q1}) + \omega L_1 \tilde{i}_{d1} + \tilde{v}_q \quad (21)$$

The voltage control loop regulates the voltage and generates the d-q axis current references for the current loop. Therefore the output of the outer voltage controller is the input of the inner control loop, a proportional-integral (PI) controller is also used in the current control loop. Then:

$$\tilde{i}_{d1-ref} = (K_{vdp} + K_{vdi}/s) (\tilde{v}_{d-ref} - \tilde{v}_d) \quad (22)$$

$$\tilde{i}_{q1-ref} = (K_{vqp} + K_{vqi}/s) (\tilde{v}_{q-ref} - \tilde{v}_q) \quad (23)$$

The second inverter operates in the power control mode, where the instantaneous values of the inverter output current components i_{d-ref} and i_{q-ref} are used to control the output active and the reactive power respectively as shown in Fig 12.

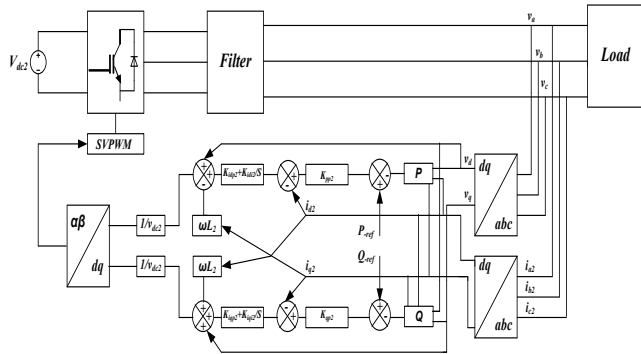


Fig. 12. The controller of the second inverter

The duty-cycle signals for the second inverter are given as:

$$\tilde{d}_{d2} \cdot V_{dc2} = (K_{idp2} + K_{idi2} / s)(\tilde{i}_{d2-ref} - \tilde{i}_{d2}) - \omega L_2 \tilde{i}_{q2} + \tilde{v}_d \quad (24)$$

$$\tilde{d}_{q2} \cdot V_{dc2} = (K_{iqp2} + K_{iqi2} / s)(\tilde{i}_{q2-ref} - \tilde{i}_{q2}) + \omega L_2 \tilde{i}_{d2} + \tilde{v}_q \quad (25)$$

In the power control mode the active and the reactive power are controlled at given set points by the outer loops to produce the d-q axis current references for the inner loops [14], [15]. The active and the reactive power are given as:

$$P = (3/2)(V_d i_{d2} + V_q i_{q2}) \quad (26)$$

$$Q = (3/2)(V_q i_{d2} - V_d i_{q2}) \quad (27)$$

The outputs of these outer controllers are the inputs of the inner control loops. A proportional (P) controller is used, then we have:

$$\tilde{i}_{d2-ref} = K_{pp2} (P_{ref} - P_2) \quad (28)$$

$$\tilde{i}_{q2-ref} = K_{qp2} (Q_{ref} - Q_2) \quad (29)$$

In order to write the closed loop equation in matrix form, new control variables are introduced into (20)-(25). Then the new duty cycle signals can be expressed as:

$$\tilde{d}_{d1} = \frac{1}{V_{dc1}} [(1 - K_{idp1} K_{vdp}) \tilde{v}_d - K_{idp1} \tilde{i}_{d1} - \omega L_1 \tilde{i}_{q1} K_{idp1} K_{vdi} \tilde{\Phi}_{d1} + K_{idi1} \tilde{v}_d + K_{idp1} K_{vdp} \tilde{v}_{d-ref}] \quad (30)$$

$$\tilde{d}_{q1} = \frac{1}{V_{dc1}} [(1 - K_{iqp1} K_{vqp}) \tilde{v}_q - K_{iqp1} \tilde{i}_{q1} + \omega L_1 \tilde{i}_{d1} K_{iqp1} K_{vqi} \tilde{\Phi}_{q1} + K_{iqi1} \tilde{v}_q + K_{iqp1} K_{vqp} \tilde{v}_{q-ref}] \quad (31)$$

$$\tilde{d}_{d2} = \frac{1}{V_{dc2}} [(1 - \frac{3}{2} K_{idp2} K_{pp2} \tilde{i}_{d2}) \tilde{v}_d - \frac{3}{2} K_{idp2} K_{pp2} \tilde{i}_{q2} \tilde{v}_q - (\frac{3}{2} K_{idp2} K_{pp2} \tilde{v}_d + K_{idp2}) \tilde{i}_{d2} - (\frac{3}{2} K_{idp2} K_{pp2} \tilde{v}_q + \omega L_2) \tilde{i}_{q2} + K_{idi2} \tilde{v}_d + K_{idp2} K_{pp2} \tilde{P}_{ref}] \quad (32)$$

$$\tilde{d}_{q2} = \frac{1}{V_{dc2}} [(1 - \frac{3}{2} K_{iqp2} K_{qp2} \tilde{i}_{d2}) \tilde{v}_q + \frac{3}{2} K_{iqp2} K_{qp2} \tilde{i}_{q2} \tilde{v}_d + (\frac{3}{2} K_{iqp2} K_{qp2} \tilde{v}_d - K_{iqp2}) \tilde{i}_{q2} - (\frac{3}{2} K_{iqp2} K_{qp2} \tilde{v}_q - \omega L_2) \tilde{i}_{d2} + K_{iqi2} \tilde{v}_q + K_{iqp2} K_{qp2} \tilde{\Phi}_{ref}] \quad (33)$$

The control output can be expressed as:

$$\tilde{\mathbf{u}} = \mathbf{H} \cdot \tilde{\mathbf{z}} + \mathbf{J} (\tilde{v}_d \tilde{v}_q \tilde{P}_{ref} \tilde{Q}_{ref}) \quad (34)$$

where; $\tilde{\mathbf{z}} = [\tilde{v}_d \tilde{v}_q \tilde{i}_{d1} \tilde{i}_{q1} \tilde{i}_{d2} \tilde{i}_{q2} \tilde{\Phi}_{d1} \tilde{\Phi}_{q1} \tilde{v}_{d1} \tilde{v}_{q1} \tilde{v}_{d2} \tilde{v}_{q2}]^T$

Substituting the control laws in the state equation and writing the equations in s-domain:

$$\mathbf{z}(s) / \mathbf{R}(s) = (s\mathbf{I} - \mathbf{A}_1 - \mathbf{B}_1 \mathbf{H})^{-1} \cdot \mathbf{B}_2 \quad (35)$$

where: $\mathbf{R}(s) = [(\tilde{v}_d \tilde{v}_q \tilde{P}_{ref} \tilde{Q}_{ref})](s)$, \mathbf{A}_1 and \mathbf{B}_1 are the state and the input matrices of the closed loop system.

4. Stability Analysis

To test the control strategy to achieve good power sharing when the DC sources are different and nonlinear a simulation using Matlab/Simulink has been carried out. The parallel inverters parameters are as follows: the capacitance and the inductance of the filters are 22 μF and 4 mH respectively. The load resistance R equals 4.25 ohm. In previous work the control parameters that achieve the optimum performance are determined [16]. The controllers' parameters are given in Table I and II.

TABLE I CONTROLLER PARAMETERS OF THE 1ST INVERTER

The Controller Parameters of the first inverter			
K_{vdp}	K_{vqp}	K_{vdi}	K_{vqi}
5	5	400	400
K_{idp1}	K_{idi1}	K_{iqp1}	K_{iqi1}
1	100	0.4	60

TABLE II CONTROLLER PARAMETERS OF THE 2ND INVERTER

The Controller Parameters of the second inverter		
K_{pp2}	K_{qp2}	K_{idp2}
5	5	1
K_{idi2}	K_{iqp2}	K_{iqi2}
100	0.4	60

In the control strategy the second inverter is forced to generate 10 kW real power and 2 kVar reactive power. Fig 13 shows that the output three phase voltages of the parallel inverters maintained at 170 V peak value. The PV arrays in Fig. 1 are denoted as A and B for the first and the second inverter respectively. In the simulation, the radiation on both arrays is fixed at 1000 W/m² while the temperature is fixed at

25 C then the radiation on the first array is reduced at 0.15 s to 800 W/m^2 . This mimics the effect of the shadow on the first array. The operating points are shown in Fig 14. The DC input voltage and current of the first inverter are shown in Fig. 15 and Fig. 16. Reducing the radiation from 1000 W/m^2 to 800 W/m^2 forces the first array to operate in new operating point. At 0.15 s when the radiation decreased to 800 W/m^2 the voltage is 427.7 V. If the operating point stays at this point then the supplied power will be less than 10 kW. Hence the operating point changes to 394 V in order to generate 10 kW. The DC input voltage and the DC input current of the second inverter are shown in Fig. 17 and Fig. 18 respectively. From the figures it can be seen that the first inverter input voltage has more oscillation than the second inverter and this is because the first inverter contains the voltage controller loop. It should be noted that most of the transient current is supplied by the first array. In the start-up a larger DC current flows in the first inverter. The small oscillation in the DC bus is because of the switching characteristics of the inverters

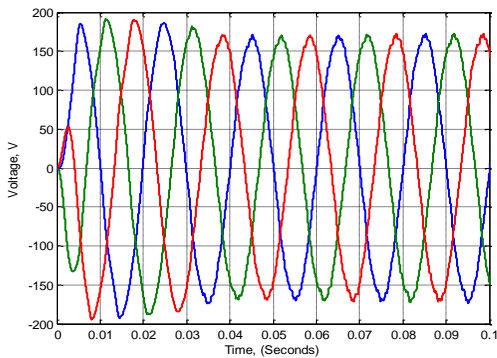


Fig. 13. The three-phase output voltage

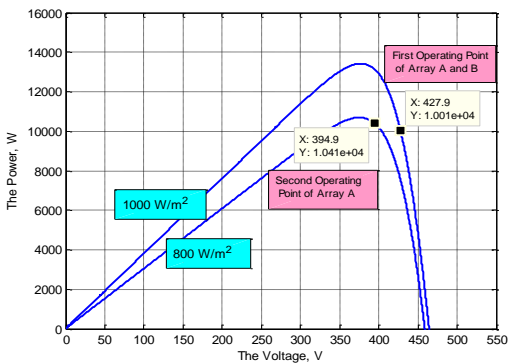


Fig. 14. The PV curve of the two arrays

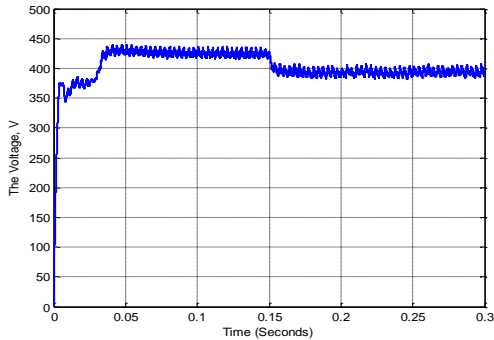


Fig. 15. The DC input voltage of the first inverter

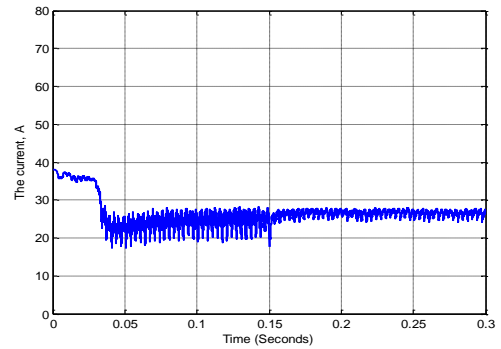


Fig. 16. The DC input current of the first inverter

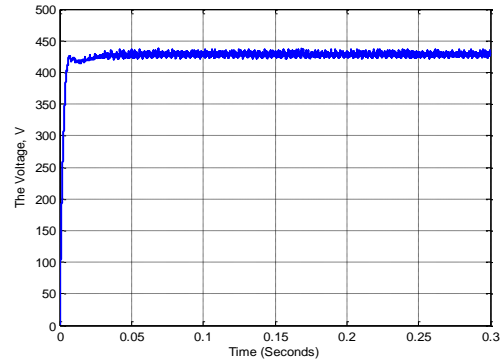


Fig. 17. The DC input voltage of the second inverter

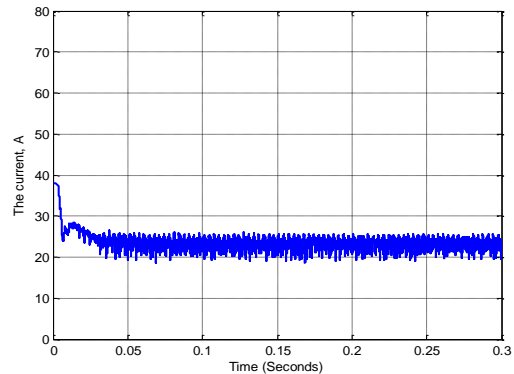


Fig. 18. The DC input current of the second inverter

The first inverter current, the second inverter and the load current are shown in Fig. 19-21. We notice there is no change in the currents at 0.15 and this is because at 800 W/m^2 the array is still capable of supplying the required power. It should be noted that at low radiation levels (500 W/m^2) the current of the first inverter is less than 40 A and since the second inverter operates in the power control mode the load power will be less than 20 kW and hence the load current will be less than 80 A. Also the peak voltage will be slightly less than 170 V. The output power of the first inverter, the second inverter and the load are shown in Fig. 22-24.

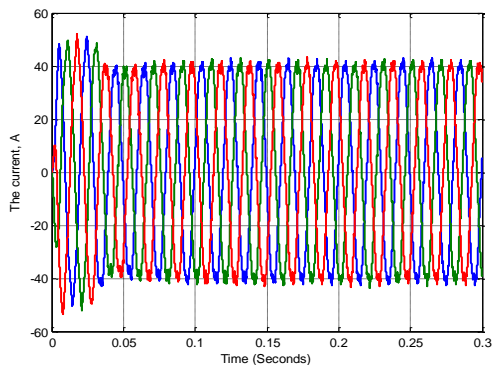


Fig 19. The output currents of the first inverter

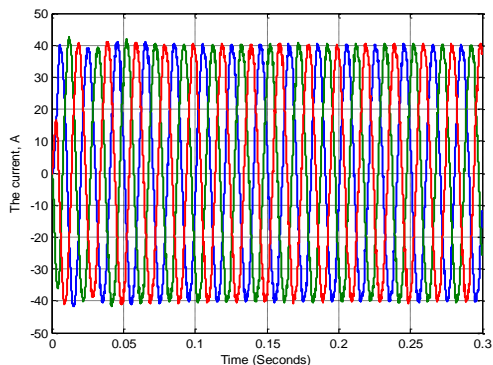


Fig. 20. The output currents of the second inverter

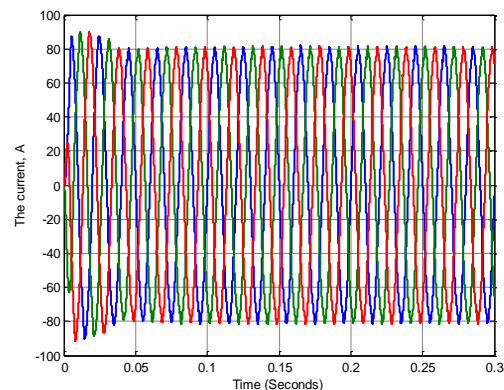


Fig. 21. The output currents of the load

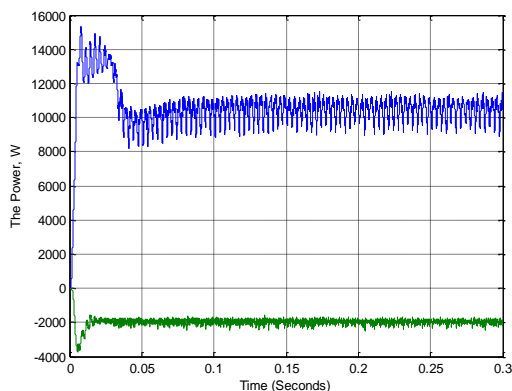


Fig. 22. The active and the reactive power of first inverter

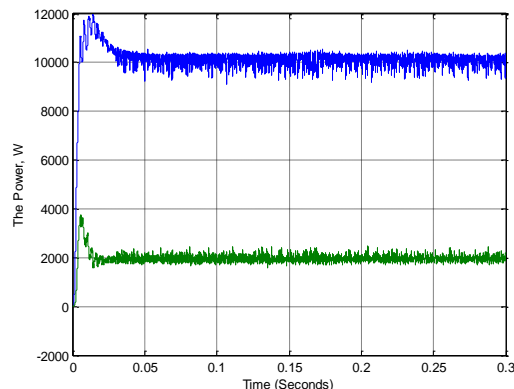


Fig. 23. The active and the reactive power of second inverter

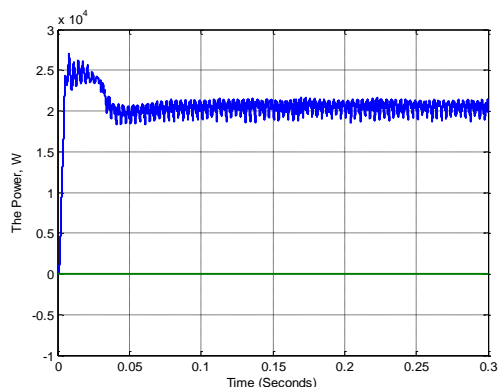


Fig. 24. The active and the reactive power of the load

As can be seen from the figures for the real and the reactive power, the reactive power supplied by the second inverter is absorbed by the first inverter. Most of the generated real power is supplied by the first inverter during transient. The system designer should take this into account and to design the PV array to be able to supply the extra power required during transient. The results show that the distributed control strategy achieves very good power sharing. The effect of the capacitor on the DC bus has been investigated and it is found that increasing the capacitor slows the system response. The simulations show that the load sharing is forced even with different nonlinear DC sources. The sharing between the inverters is good even during the transient but the first inverter supplies most of the current. In the simulation the nonlinear model of the inverters is implemented. The work in this paper is to be extended to deal with stability analysis with time delay and data loss where the control signals are exchanged through shared communication network [17]. Additionally the distributed control strategy will be tested when the DC sources comes from different renewable sources.

5. Conclusion

In this paper the modelling and control of PV-based Microgrid is presented. The PV-based Microgrid if formed by two voltage source inverters each is fed with 10 kWp PV array. The small-signal model for the parallel inverters and the PV array is briefly described. The distributed control strategy in the d-q frame is implemented where the first inverter controller contains voltage control loop and current

control loop. The second inverter controller works in the power control mode. The PV array, the two inverters and their controller are implemented in Matlab/Simulink. As the PV array is a nonlinear and variable DC source the controller is designed to achieve power sharing even with different DC nonlinear sources. The controller is tested and the power sharing is achieved even when the two PV arrays receive different radiation. With this distributed control strategy the first inverter supplies most of the current during the transient. The current research is to test the controller strategy with different renewable sources such as wind turbines and fuel cells.

References

- [1] Lasseter, B., 2001. "Microgrids [distributed power generation]", In Proceedings of 2001 Winter Meeting of the IEEE Power Engineering Society, 28 Jan.-1 Feb, Piscataway, NJ, USA: IEEE, pp. 146-149.
- [2] Friederike Kersten, Roland Doll, Andreas Kux, Dominik M.Huljic, Marzella A.Gorig, Christian Breyer, Jorg W.Müller, and Peter Wawer, "PV Learning Curves: Past and Future Drivers Of Cost Reduction", In the Proceedings of the 26th European Photovoltaic Solar Energy Conference, 5-9 September, Germany: 2011, .
- [3] Prodanovic, M., Green, T.C., & Mansir, H. . "Survey of control methods for three-phase inverters in parallel connection". In the Proceedings of the 8th IEEE Conference on Power Electronics and Variable Speed Drives, 2000, pp.) 472-477.
- [4] De Brabandere, K., Bolsens, B., Van den Keybus, J., Woyte, A., Driesen, J., Belmans, R., & Leuven, K. U., 2004. "A voltage and frequency droop control method for parallel inverters", In 2004 IEEE 35th Annual Power Electronics Specialists Conference, 20-25 June, Piscataway, NJ, USA: IEEE, pp. 2501-2507.
- [5] Mazumder, S.K., Tahir, M., & Acharya, K. 2008. "Master-slave current-sharing control of a parallel dc-dc converter system over an RF communication interface". IEEE Transactions on Industrial Electronics, 55, (1) 59-66.
- [6] Mazumder, S.K., Tahir, M., & Acharya, K. 2010. "An Integrated Modeling Framework for Exploring Network Reconfiguration of Distributed Controlled Homogenous Power Inverter Network using Composite Lyapunov Function Based Reachability Bound". Simulation, 86, (2) 75-92
- [7] Wei, Y., Zhang, X., Qiao, M., & Kang, J. "Control of parallel inverters based on CAN bus in large-capacity motor drives", In 2008 Third IEEE International Conference on Electric Unity Deregulation, 6-9 April 2008, Piscataway, NJ, USA: IEEE, pp. 1375-1379
- [8] Yai Zhang, Hao Ma and Fei Xu, "Study on Networked Control for Power Electronic Systems", In the Proceedings of the Power Electronics Specialists Conference, 17-21 June, Orlando, FL, USA, pp. 833-838.
- [9] J. A. Gow, C. D. Manning, "Development of a photovoltaic array model for use in power-electronics simulation studies", IEE Proceedings-Electric Power Applications, Vol 146, No. 2, pp. 193-200, 1999.
- [10] G. Walker, "Evaluating MPPT Converter Topologies Using a Matlab PV Model", Journal of Electrical and Electronics Engineering, Australia, Vol. 21, No. 1, pp. 49-56, 2001.
- [11] Hansen A. D., Sorensen P., Hansen L. H., Binder H., "Model for stand-alone PV system", Roskilde: Rio National Laboratory, 2000.
- [12] Solarex MSX60 datasheet. Available online at: <http://www.californiasolarcenter.org/newssh/pdfs/Solarex-MSX64.pdf>
- [13] Zhihong Ye, "Modeling and Control of Parallel Three-Phase PWM Converters", PhD thesis, Virginia State University, September 15, 2000.
- [14] Yu Zhang, "Small-Signal Modeling and Analysis of Parallel- Connected Power Converter Systems for Distributed Energy Resources" PhD thesis, University of Miami, 2011.
- [15] Yu Zhang, Zhenhua Jiang, and Xunwei Yu, "Small-Signal Modeling and Analysis of Parallel-Connected Voltage Source Inverters" In the proceedings of the IEEE 6th confenrence on Power Electronic and Motion Control, pp. 377-383, May 17-20, 2009.
- [16] A. F. Khalil, Khalid Ateea and Ahmed El-Barsha, "Stability Analysis of Parallel Inverters Microgrid", The 20th International Conference on Automation and Computing (IEEE), UK, September 2014, pp. 110-115.
- [17] A. F. Khalil and J. Wang, "Estimation of Maximum Allowable Time-Delay Bound for System Stability of Network Controlled Parallel DC/DC Buck Converters," The 18th International Conference on Automation and Computing (IEEE), Loughborough, UK September 2012, pp. 1-6.